energies

MDPI

Article

A New Method for State of Charge Estimation of Lithium-Ion Battery Based on Strong Tracking Cubature Kalman Filter

Bizhong Xia [1], Haiqing Wang [1,*], Mingwang Wang [2], Wei Sun [2], Zhihui Xu [2] and Yongzhi Lai [2]

Received: 3 October 2015; Accepted: 18 November 2015; Published: 26 November 2015
Academic Editor: K.T. Chau

[1] Graduate School at Shenzhen, Tsinghua University, Shenzhen 518055, China; xiabz@sz.tsinghua.edu.cn
[2] Sunwoda Electronic Co. Ltd., Shenzhen 518108, China; lyz@sunwoda.com (M.W.); sunwei@sunwoda.com (W.S.); luojie@sunwoda.com (Z.X.); dahai17@126.com (Y.L.)
* Correspondence: wanghq14@mails.tsinghua.edu.cn; Tel./Fax: +86-0755-2603-6982

Abstract: The estimation of state of charge (SOC) is a crucial evaluation index in a battery management system (BMS). The value of SOC indicates the remaining capacity of a battery, which provides a good guarantee of safety and reliability of battery operation. It is difficult to get an accurate value of the SOC, being one of the inner states. In this paper, a strong tracking cubature Kalman filter (STCKF) based on the cubature Kalman filter is presented to perform accurate and reliable SOC estimation. The STCKF algorithm can adjust gain matrix online by introducing fading factor to the state estimation covariance matrix. The typical second-order resistor-capacitor model is used as the battery's equivalent circuit model to dynamically simulate characteristics of the battery. The exponential-function fitting method accomplishes the task of relevant parameters identification. Then, the developed STCKF algorithm has been introduced in detail and verified under different operation current profiles such as Dynamic Stress Test (DST) and New European Driving Cycle (NEDC). Making a comparison with extended Kalman filter (EKF) and CKF algorithm, the experimental results show the merits of the STCKF algorithm in SOC estimation accuracy and robustness.

Keywords: strong tracking cubature Kalman filter; state of charge; lithium-ion battery; electric vehicle

1. Introduction

In recent years, energy-saving and emission reduction attract special attentions and environmental pollution have become more and more critical. Electric vehicles (EVs), characterized by environmentally benign property and zero-emissions, are with people's horizons. Research and development on electric vehicle batteries have been greatly active, especially because of the increasing cost of energy consumption. Lithium-ion batteries conform to the demands of EVs and hybrid electric vehicles (HEVs) for their high energy density, safety, low self-discharge and long cycle life. The system that regulates the energy flow in a battery pack with respect to voltages of individual cells, temperature, state of charge and health is defined as the Battery Management System (BMS) [1,2]. The main task of BMS is to maintain a safe operating environment for the battery system, and to protect it from damage. The state of charge (SOC), defined as the ratio of the remaining capacity to the rated capacity, is the core part of BMS. An accurate SOC estimation prevents over-charging or over-discharging time and prolongs the life of batteries on the one hand, and, on the other hand, it helps drivers effectively grasp running condition of their electric vehicle. Because the SOC is

sensitively influenced by discharge rate, ambient temperature, and aging degree of the battery, the accurate value of the SOC is difficult to obtain.

To predict precise SOC values, numerous SOC estimation methods have been proposed, like Ampere-hour (Ah) counting method [3], open-circuit voltage (OCV) method [4], artificial neural network (ANN) [5,6], particle filter (PF) [7,8], a series of algorithms based on Kalman filter [9–17]. The Ah counting method is the most common technique for the battery SOC determination in practice. The main idea of the method is integrating the current. However, this method dissatisfies estimation accuracy requirement because of initial value errors and the integral accumulation error caused by measurement current. The OCV method uses the relationship between the open circuit voltage and the SOC for the specific battery type, then, the SOC value can be obtained with interpolation method. However, this method is improper for online applications since the battery has to be left in open circuit mode for a long time to reach the steady-state before measuring the OCV. In addition, some kinds of batteries do not have a definite relationship between OCV and SOC, such as lithium iron phosphate batteries, which have voltage plateaus. Nevertheless, the method is effective for determining the SOC at the initial and end stages due to its simplicity. The ANN method predicts the SOC according to the nonlinear relationship between the battery SOC and its influencing factors obtained by the trained black-box battery models. This method has excellent performance if the training data is sufficient to cover the total loading conditions. Nevertheless, it is time-consuming and nearly impossible to collect training data covering all of the battery loading conditions. The PF method needs numerous matrix operations and has high requirement for hardware.

Recently, a widely used method, Kalman filter (KF) [9] algorithm, which is originally developed to optimize the estimate state for linear systems, is applied to predict the battery SOC. The aim of the algorithm is to extract accurate information out of noisy measurements, and then correct it. Since lithium-ion batteries are a nonlinear system, extended Kalman filter (EKF) [10–13] and unscented Kalman filter (UKF) methods [15–17] have been developed to solve this problem. The EKF use a linearization process, namely a first-order Taylor series expansion, at every time step to approximate the nonlinear system. However, the instability of the filter and the lack of robustness due to the linearization process, and also the nontrivial, error-prone calculation of the Jacobian matrices can be listed as the shortcomings of the EKF approach. As an alternative, sigma-point Kalman filters (SPKF) have higher order accuracy in the error covariance of the state vector compared to EKF. The SPKF-based methods are comparable in terms of complexity with Jacobian matrix deploying EKF [14], moreover, achieving a second-order accuracy compared to EKF's first order accuracy at the same complexity level is important to note [15]. The UKF introduces an unscented transformation to approximate the state distribution through a set of sample points called sigma points. It has been demonstrated that UKF has better performance than EKF in terms of accuracy and robustness. Even so, despite its derivative-free state estimation, the standard UKF has the possibility to suffer from performance degradation and instability problems in the case of a mismatch between the *a priori* assumptions, which include an accurate model, proper initial values and full information of the noise distribution.

Many electrochemical model-based approaches [18–20], which are derived from principles of electrochemistry, are proposed get precise knowledge of battery internal information like SOC. In [18], two nonlinear robust observer designs have been presented for SOC estimation of Li-ion cells using an uncertain reduced electrochemical model. Simulation studies and experiments are presented to show the effectiveness of the observer designs. According to [19], an adaptive observer design based on a coupled electrochemical-thermal model, is presented for simultaneous state-parameter estimation of a Li-ion cell. Simulation studies show the effectiveness of the design where the states and parameters are estimated with a desired convergence rate and accuracy. Although electrochemical model-based techniques are arguably more accurate than the other modeling approaches, the complexity and computation cost will increase accordingly.

In 2009, a new nonlinear filter based on KF called as cubature Kalman filter (CKF) was proposed by Arasaratnam and Haykin [21]. The key idea of this method is using the radial-spherical cubature rule to capture the mean and covariance of the states of a nonlinear system with additive Gaussian noise. The CKF uses a set of $2n$ points to predict the SOC of the battery, while the UKF uses a set of $2n + 1$ points, where n represents the state-vector dimension. It has already been proven more accurate and stable than the UKF [22,23]. The CKF has been successfully applied in many fields, such as moving-target tracking [24] and spacecraft attitude estimation [25].

In this paper, a new strong tracking cubature filter (STCKF) method for SOC estimation is presented to improve the robustness and accuracy of the CKF method. Two typical driving cycles, including Dynamic Stress Test (DST) and NEDC, are applied to assess the performance of the proposed method. The experimental results show that this method can obtain super performance in terms of accuracy and robustness, better than EKF and CKF.

The remainder of this paper is organized as follows. In Section 2, the second-order resistor-capacitor equivalent circuit model is used and the model parameters are determined by exponential-function fitting method. The CKF and STCKF methods are illustrated in detail in Section 3. Section 4 describes the experimental configurations. The verification results and comparisons of different approaches are discussed in Section 5, and conclusions of the paper are made in Section 6.

2. Battery Model and Parameters Identification

2.1. Battery Model

Equivalent circuit models, which consist of basic circuit elements (e.g., resistors, capacitors and inductors), are commonly used to simulate the voltage-current behaviors of a battery [26–28]. Building an effective equivalent circuit model (ECM) makes a great difference for researching battery management system. Estimation accuracy is certainly based on the precise ECM for SOC estimation algorithms. Then, the application of ECM prevents batteries from unnecessary and permanent damage in actual operation.

When choosing ECM, the following several aspects must be considered. First of all, the model can clearly imitate the dynamic behaviors of the battery. Secondly, it must not be too complicated to establish the state-space equations so complex computations do not increase the burden on the CPU. The complicated ECM can well simulate dynamic behaviors while it increases the computation cost. Therefore, a tradeoff must be made to meet the above requirements.

Hence, this paper is based on a second-order equivalent circuit battery model. As shown in Figure 1, the second-order RC battery model consists of an open-circuit voltage $U_{oc}(SOC)$ that has a certain relationship with SOC at the same temperature, a resistor R_o, and two parallel resistor-capacitor (RC) networks connected in series (*i.e.*, R_1-C_1 and R_2-C_2). The resistor R_o is the ohmic resistance caused by the accumulation and dissipation of charge in the electrical double-layer, R_1 and C_1 are the activation polarization resistance and capacitance, respectively, while R_2 and C_2 separately are the concentration polarization resistance and capacitance, respectively.

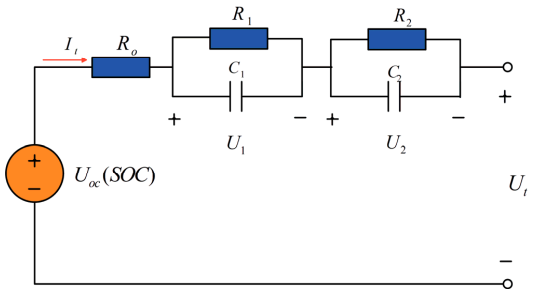

Figure 1. Schematic diagram of the second-order resistor-capacitor (RC) equivalent circuit model.

The cell SOC is defined as the coefficient of the remaining capacity to the nominal capacity. The SOC can be expressed as the following equation:

$$SOC(t) = SOC(t_0) - \frac{\int_{t_0}^{t} i(t)dt}{Q_N} \tag{1}$$

where $i(t)$ represents the value of current (defined to be negative for discharging and positive for charging). Q_N is the nominal capacity. $SOC(t_0)$ represents the SOC value at time t_0.

The derivation of SOC based on Equation (1) can be formulated as:

$$SOC'(t) = -\frac{i(t)}{Q_N} \tag{2}$$

According to the circuit theory, the electrical behavior of the second-order RC battery model can be expressed as:

$$\begin{cases} SOC'(t) = -\frac{i(t)}{Q_N} \\ U_1' = -\frac{U_1}{R_1C_1} + \frac{1}{C_1}i(t) \\ U_2' = -\frac{U_2}{R_2C_2} + \frac{1}{C_2}i(t) \end{cases} \tag{3}$$

$$U_t = U_{oc}(SOC) - U_1 - U_2 - R_o i(t) \tag{4}$$

where U_1 and U_2 denote the terminal voltage of C_1 and C_2, respectively; and U_t and $i(t)$ denote individually the value of terminal voltage and current, respectively. U_{oc} denotes the open-circuit voltage, which is usually a nonlinear function of SOC at the same temperature.

2.2. Parameters Identification

For the second-order RC equivalent circuit model indicated in Figure 1, the value of parameters $\{U_{oc}(SOC), R_o, R_1, R_2, C_1, C_2\}$ and the relationship between OCV and SOC have to be identified. These parameters can be divided into two parts. The first part is U_{oc}, which has a certain relationship with SOC. The second is comprised of $\{R_o, R_2, R_2, C_1, C_2\}$, which describe the dynamic behaviors of battery. To identify these parameters, some experiments have been carried out on the ICR18650-22F lithium-ion battery (Samsung, Seoul, Korea).

To collect data for determining the relationship of OCV *versus* SOC, a consecutive test was performed on the battery. First, the battery is charged to the fully charged state with the standard charging pattern and fully discharged at the same temperature twice. Then, after 2 h rest, the fully charged battery that has reached steady state is discharged with a constant current of 0.1 C by 10% of the nominal capacity and it is left in the open-circuit for condition for 5 h. Repetitive operation of the above discharging with a constant current and rest is executed until the batter achieves the fully discharged state. The entire process of experiment is presented in Figure 2.

According to the measured data from the above test, sixth-order polynomial fitted curve are shown in Figure 3, which can well describe the nonlinear relationship between the OCV and the SOC:

The exponential-function fitting method [28–30] is adopted to identify parameters $\{R_o, R_2, R_2, C_1, C_2\}$. The details of parameters identification can be found in [29], which has been published by our research group.

The identified parameters of second-order RC ECM are listed in Table 1.

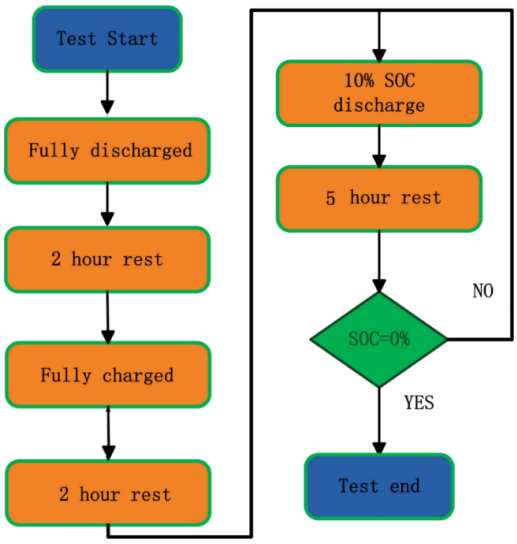

Figure 2. Flow chart of an open-circuit voltage (OCV) test for determining the relationship of OCV and state of charge (SOC).

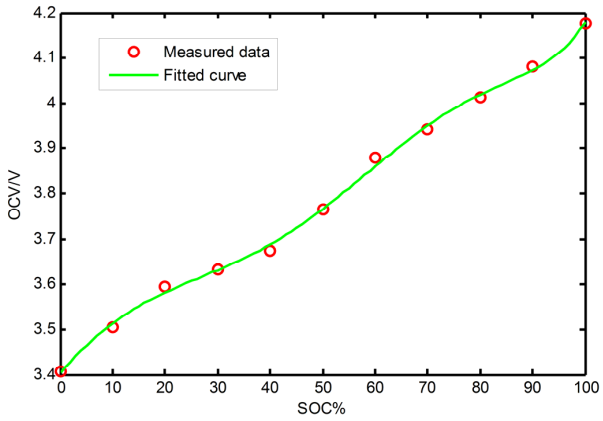

Figure 3. The sixth-order polynomial fitted curve between OCV and SOC.

Table 1. Identified parameters of second-order RC ECM.

Parameters	R_o	R_1	R_2	C_1	C_2
Value	0.0377 Ω	0.0242 Ω	0.00300 Ω	1673.3 F	17,823 F

3. SOC Estimation Based on the Strong Tracking Cubature Kalman Filter

3.1. Cubature Kalman Filter Algorithm (CKF)

In 2009, a new nonlinear filter called the cubature Kalman filter (CKF) [21,22] was proposed by Arasaratnam and Haykin. On the basis of the Bayesian filter, the CKF uses a set of $2n$ points to capture the mean and covariance of the states with additive Gaussian noise by the three-degree radial-spherical cubature rule.

The basic idea of the Bayesian filter is calculating the multi-dimensional weighted integral, which can be expressed as:

$$I(f) = \int_D f(x)w(x)dx \tag{5}$$

where $f(\cdot)$ is some nonlinear function, $D \in R^n$ is the region of integration, and the known weighting function $w(x) \geqslant 0$ for all $x \in D$. In a Gaussian-weighted integral, $w(x)$ is a Gaussian density and satisfies the non-negativity condition in the entire region. According to [21], it can be obtained that:

$$\begin{gathered} I(f) = \int_D f(x)N(x;0,I)dx \approx \sum_{i=1}^{2n} w_i f(\xi_i) \\ \xi_i = \sqrt{n}[1]_i, w_i = \frac{1}{2n} \quad i = 1,2,\cdots\cdots,2n \end{gathered} \tag{6}$$

where $N(x;\ 0,\ I)$ is Standard Gaussian distribution, n represents the state-vector dimension, $[1]_i$ represents the i-th column vector. The third-degree cubature rule is exact for Gaussian-weighted integrals whose integrands are written in the form of a linear combination of monomials up to the third degree.

A discrete-time nonlinear dynamical system with additive process and measurement noises is as follows:

$$\begin{cases} x_{k+1} = f(x_k, u_k) + \Gamma_k w_k \\ y_{k+1} = h(x_k, u_k) + v_k \end{cases} \tag{7}$$

where $X_k \in R^n$ is the state vector at time k; $y_k \in R^m$ is the measurement vector at time k; $f(\cdot)$ and $h(\cdot)$ are known nonlinear functions; Γ_k is the discrete-time process noise distribution matrix; $\boldsymbol{w_k}$ and $\boldsymbol{v_k}$ are independent Gaussian white process noise and measurement noise with covariance Q_k and R_k separately.

The process of the CKF algorithm for battery SOC estimation is summarized as follows.

(a) Initialization:

$$\hat{x}_0 = E[x_0],\ P_0 = E[(x_0 - \hat{x}_0)(x_0 - \hat{x}_0)^T] \tag{8}$$

(b) Time update

(1) Calculate the cubature points:

$$P_k = S_k {S_k}^T \tag{9}$$

$$x^i{}_k = S_k \xi_i + \hat{x}_k \quad i = 1,2,\cdots\cdots,2n \tag{10}$$

where n represents the state-vector dimension and ξ is the set of standard cubature points, which is shown by:

$$\xi_i = \begin{cases} \sqrt{n}[1]_i & i = 1,2,\cdots,n \\ -\sqrt{n}[1]_i & i = n+1, n+2,\cdots,2n \end{cases}$$

where $[1]_i$ represents the identity matrix and $[1]^{(i)}$ denotes its i-th column vector.

(2) Calculate the propagated cubature points:

$$\chi^i_{k+1|k} = f({x_k}^i) \tag{11}$$

(3) Calculate the predicted state and covariance:

$$\hat{x}_{k+1|k} = \frac{1}{2n}\sum_{i=1}^{2n} \chi^i_{k+1|k} \tag{12}$$

$$P_{k+1|k} = \frac{1}{2n}\sum_{i=1}^{2n} \chi^i{}_{k+1|k}(\chi^i{}_{k+1|k})^T - \hat{x}_{k+1|k}(\hat{x}_{k+1|k})^T + Q_k \tag{13}$$

where Q_k is the process noise covariance matrix at time step k.

(c) Measurement update

(1) Calculate the cubature points:

$$P_{k+1|k} = S_{k+1|k} {S_{k+1|k}}^T \tag{14}$$

$$x^i{}_{k+1|k} = S_{k+1|k}\xi_i + \hat{x}_{k+1|k} \tag{15}$$

(2) Calculate the propagated cubature points:

$$y_{k+1}{}^i = h(x^i{}_{k+1|k}) \tag{16}$$

(3) Calculate the predicted measurement and covariance:

$$\hat{y}_{k+1} = \frac{1}{2n}\sum_{i=1}^{2n} y_{k+1}{}^i \tag{17}$$

$$P^y{}_{k+1} = \frac{1}{2n}\sum_{i=1}^{2n} y^i{}_{k+1}(y^i{}_{k+1})^T - \hat{y}_{k+1}(\hat{y}_{k+1})^T \tag{18}$$

$$P^{xy}{}_{k+1} = \frac{1}{2n}\sum_{i=1}^{2n} x^i{}_{k+1}(x^i{}_{k+1})^T - \hat{x}_{k+1|k}(\hat{x}_{k+1|k})^T \tag{19}$$

where R_k is the measurement noise covariance matrix at time step k.

(d) Estimate the Kalman gain, updated state and error covariance:

$$K_{k+1} = P^{xy}{}_{k+1}(P^y{}_{k+1})^{-1} \tag{20}$$

$$\hat{x}_k = \hat{x}_{k+1|k} + K_{k+1}(y_{k+1} - \hat{y}_{k+1}) \tag{21}$$

$$P_{k+1} = P_{k+1|k} - K_{k+1}P^y{}_{k+1}{K_{k+1}}^T \tag{22}$$

3.2. Strong Tracking Cubature Kalman Filter (STCKF)

Although the EKF has been widely used, it is limited for the following drawbacks:

(1) Poor robustness against model uncertainties.
(2) Loss of tracking ability for sudden changes of the state when it has reached steady state.
(3) Cannot be used to estimate time-varying parameters.

In order to improve performance of EKF, strong tracking filter (STF) was proposed [31,32] and used for battery SOC estimation [33]. In the actual design, STF still continues to use framework of Kalman filter because of conciseness and recursive property. The framework of Kalman filter can be expressed as:

$$\hat{x}_k = \hat{x}_{k+1|k} + K_{k+1}\gamma_{k+1} \tag{23}$$

$$\gamma_{k+1} = (y_{k+1} - H_{k+1}\hat{x}_{k+1|k}) \tag{24}$$

where γ_{k+1} is residual sequence of measurement. H_k is $H_k = \left.\frac{\delta h(x_k)}{\delta x_k}\right|_{x_k=\hat{x}_k}$ when the system is nonlinear. Hence, STF is transformed into seeking the optimal filter gain matrix K_{k+1} that can be deduced by orthogonality principle [32–34].

$$E[(x_{k+1} - \hat{x}_{k+1})(x_{k+1} - \hat{x}_{k+1})^T] = \min \tag{25}$$

$$V_{j,k+1} = E[\gamma_{k+1}{\gamma_{k+1}}^T] = 0 \tag{26}$$

When system model and real system completely match and modeling error does not exist, residual sequence of Kalman filter output is white Gaussian noise with zero mean, so these residual

sequences are mutually orthogonal. Equation (25), which is the performance index of Kalman filter, denotes the minimum error estimation covariance and Equation (26) represents that these residual sequences are mutually orthogonal. Since the system model is not very accurate in fact, the mean of residual sequence will show this problem when state estimation of filter deviates from the system state. Thus, the STF can adjust gain matrix online by introducing fading factor to the state estimation covariance matrix.

$$P_{k+1|k} = \lambda_{k+1} P^{x}_{k+1|k} + Q_k \tag{27}$$

where λ_{k+1} is the fading factor; $P^{x}_{k+1|k}$ is state estimation covariance matrix before introducing fading factor; $P_{k+1|k}$ is state estimation covariance matrix after introducing fading factor; Q_k is covariance of process noise. The fading factor can be obtained by following equations:

$$\gamma_{k+1} = (y_{k+1} - \hat{y}_{k+1}) \tag{28}$$

$$V_{0,k+1} = \begin{cases} \gamma_1 {\gamma_1}^T & \text{k=0} \\ \frac{\rho V_{0,k} + \gamma_{k+1} {\gamma_{k+1}}^T}{1+\rho} & \text{k} \geqslant 1 \end{cases} \tag{29}$$

$$N_{k+1} = V_{0,k+1} - H_k Q_k {H_k}^T - \beta R_{k+1} \tag{30}$$

$$M_{k+1} = H_{k+1} F_k P_k {F_k}^T {H_k}^T \tag{31}$$

$$\lambda_0 = \frac{tr\left[N_{k+1}\right]}{tr\left[M_{k+1}\right]} \tag{32}$$

$$\lambda_{k+1} = \max(1, \lambda_0) \tag{33}$$

where H_k and F_k are the measure matrix and process matrix, respectively, and λ_k is called the fading factor which adjusts gain matrix to realize orthogonality principle. Q_k and R_k are covariance of process noise and measure noise, respectively. The matrix N_{k+1} and M_{k+1} are defined by Equations (30) and (31), which are used for calculating the fading factor λ_k; $tr[N_k]$ and $tr[M_k]$ are the trace of matrix N_k and M_k, respectively.

By combining the above cubature Kalman filter and strong tracking filter, we can deduce the strong tracking cubature Kalman filter (STCKF) algorithm in detail, as shown in Table 2.

In Table 2, after initialization, the estimated state vector $\hat{x}_{k+1|k}$ and the estimation error covariance $P_{k+1|k}$ can be firstly achieved according to the time and measurement update processes. Then, the fading factor λ_{k+1} is calculated. The estimated state vector $\hat{x}_{k+1}$ and the estimation error covariance P_{k+1} after adding the fading factor are obtained though update processes. $\hat{x}_{k+1}$, P_{k+1} and λ_{k+1} are used for the next prediction and update processes. The battery SOC can be recursively estimated by repeating the above procedure.

Table 2. Summary of strong tracking cubature Kalman filter (STCKF) algorithm.

Initialization	$\hat{x}_0 = E[x_0],\ P_0 = E[(x_0 - \hat{x}_0)(x_0 - \hat{x}_0)^T]$
(1) Time update	
(a) The cubature points	$P_k = S_k {S_k}^T, {x^i}_k = S_k \xi_i + \hat{x}_k$
(b) Propagated cubature points	${\chi^i}_{k+1|k} = f({x^i}_k)$
(c) State and covariance time update	$\hat{x}_{k+1|k} = \frac{1}{2n} \sum_{i=1}^{2n} {\chi^i}_{k+1|k}$ ${P^x}_{k+1|k} = \frac{1}{2n} \sum_{i=1}^{2n} {\chi^i}_{k+1|k} ({\chi^i}_{k+1|k})^T - \hat{x}_{k+1|k} \hat{x}^T_{k+1|k} + Q_k$ ${P^l}_{k+1|k} = {P^x}_{k+1|k} + Q_k$

Table 2. *Cont.*

Initialization	$\hat{x}_0 = E[x_0],\ P_0 = E[(x_0 - \hat{x}_0)(x_0 - \hat{x}_0)^T]$
(2) Measurement update	
(a) The cubature points	$P^l{}_{k+1\|k} = S^l_{k+1\|k} S^l_{k+1\|k}{}^T$ $x^{i,l}_{k+1\|k} = S^l_{k+1\|k}\xi_i + \hat{x}_{k+1\|k}$
(b) Propagated cubature points	$\gamma^{i,l}_{k+1} = h(x^{i,l}_{k+1\|k})$
(c) Measurement and error covariance	$\hat{y}_{k+1} = \frac{1}{2n}\sum_{i=1}^{2n} \gamma^{i,l}_{k+1}$ $P^{xy,l}_{k+1\|k} = \frac{1}{2n}\sum_{i=1}^{2n} x^{i,l}{}_k(\gamma^{i,l}_{k+1})^T - \hat{x}_{k+1\|k}\hat{y}^T_{k+1}$
(3) The fading factor	$\lambda_{k+1} = \max(1, \lambda_0)$ $\lambda_0 = \frac{tr[N_{k+1}]}{tr[M_{k+1}]}$ $N_{k+1} = V_{0,k+1} - H_k Q_k H_k{}^T - \beta R_{k+1}$ $M_{k+1} = H_{k+1} F_k P_k F_k{}^T H_k{}^T$ $V_{0,k+1} = \begin{cases} \gamma_1 \gamma_1{}^T & \text{k=0} \\ \frac{\rho V_{0,k} + \gamma_{k+1}\gamma_{k+1}{}^T}{1+\rho} & \text{k} \geqslant 1 \end{cases}$
(4) Update after add fading factor	
(a) The cubature points	$P_{k+1\|k} = \lambda_{k+1} P^x_{k+1\|k} + Q_k$ $x^i_{k+1\|k} = S_{k+1\|k}\xi_i + \hat{x}_{k+1\|k}$
(b) Propagated cubature points	$\gamma^i_{k+1} = h(x^i_{k+1\|k})$
(c) Measurement and error covariance	$\overline{y}_{k+1} = \frac{1}{2n}\sum_{i=1}^{2n} \gamma^i_{k+1}$ $P^y_{k+1} = \frac{1}{2n}\sum_{i=1}^{2n} \gamma^i_{k+1}(\gamma^i_{k+1})^T - \overline{y}_{k+1}\overline{y}_{k+1}{}^T$ $P^{xy}_{k+1} = \frac{1}{2n}\sum_{i=1}^{2n} x^i_{k+1\|k}(\gamma^i_{k+1})^T - x_{k+1\|k}\overline{y}_{k+1}{}^T$
(d) Estimate the Kalman gain, updated state and error covariance	$K_{k+1} = P^{xy}_{k+1}(P^y_{k+1})^{-1}$ $\hat{x}_{k+1} = \hat{x}_{k+1\|k} + K_{k+1}(y_{k+1} - \hat{y}_{k+1})$ $P_{k+1} = P_{k+1\|k} - K_{k+1} P^y_{k+1} K^T_{k+1}$

4. Experimental Configurations

Figure 4 shows the schematic of battery test bench. It consists of (1) tested Samsung lithium-ion batteries; (2) a control board for controlling battery charge/discharge, as well as battery voltage and current sampling with a period of 1 s; (3) a host computer with monitoring software for data sampling and MATLAB R2010a for data analysis; (4) a DC contactor for charge/discharge switching; (5) a programmable power supply for cell charging; and (6) a programmable electric load for cell discharging. The $LiNi_xCo_yMn_zO_2$ ($x + y + z = 1$) lithium-ion battery, which will be the next generation of the mainstream batteries for EVs, has a distinctive features in energy density, power density, cycle life and so on. The batteries used in this test are Samsung ICR18650-22P lithium-ion battery, whose nominal capacity and nominal voltage are 2.2 Ah and 3.62 V, respectively.

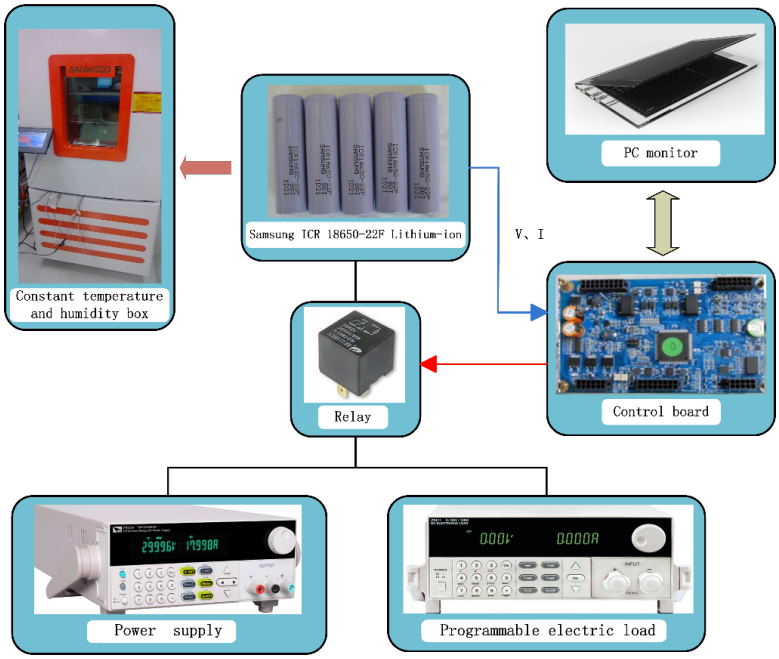

Figure 4. Schematic of battery test bench.

5. Verification Results and Analysis

5.1. Estimation Results under Dynamic Stress Test (DST) Cycle

A good SOC estimation technique should be able to perform effectively under different loading profiles. Thus, we collected battery discharge data using dynamic stress testing (DST) to verify the applicability of the developed method during working conditions, which is a step charge/discharge profile. The current profile and zoom profile for DST are shown in Figure 5a,b, respectively.

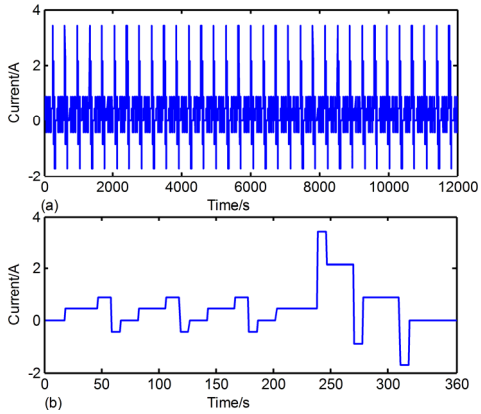

Figure 5. Dynamic Stress Testing: (**a**) current profile and (**b**) zoom plot of current profile.

The estimation curve of SOC is presented in Figure 6a, where the black dotted-line is the reference SOC values computed using Coulomb counting method with accurate current values and initial SOC value, while the red solid-line and black solid-line is the estimated results with STCKF and EKF method, respectively. The initial SOC value for STCKF and EKF method was set at 95% for two reasons: (1) to simulate preferably the actual conditions, where the exact SOC at the beginning of usage is unknown or inaccurate, and (2) to measure the self-correction capability of the STCKF method. The SOC estimation error of STCKF and EKF method is indicated in Figure 6b with the red

solid-line and black solid-line. From Figure 6c, we can easily get that the value of SOC estimation error with STCKF is a little bigger than the result with EKF method at the beginning. Then, SOC estimation error deceases and approaches a very small value gradually; however, estimation error using EKF method changes little. The SOC estimation error from 4000 to 5000 s is shown in Figure 6c, which indicates that the maximum error of STCKF is less than 1% and the maximum error of EKF is about 3%. The battery terminal voltage *versus* time is shown in Figure 7a, where the blue solid-line is the measured terminal voltage with a high precision voltage sensor and the red dotted-line is the estimated voltage by the developed method. It can be seen that the terminal voltage shows serious fluctuations due to the sharply variable current. However, the voltage estimation error has small fluctuations and the average value of estimation error is about 0.02 V, as shown in Figure 7b. The estimation results of SOC and terminal voltage illustrate that the proposed method for SOC estimation has good performance in terms of estimation accuracy and self-correction capability.

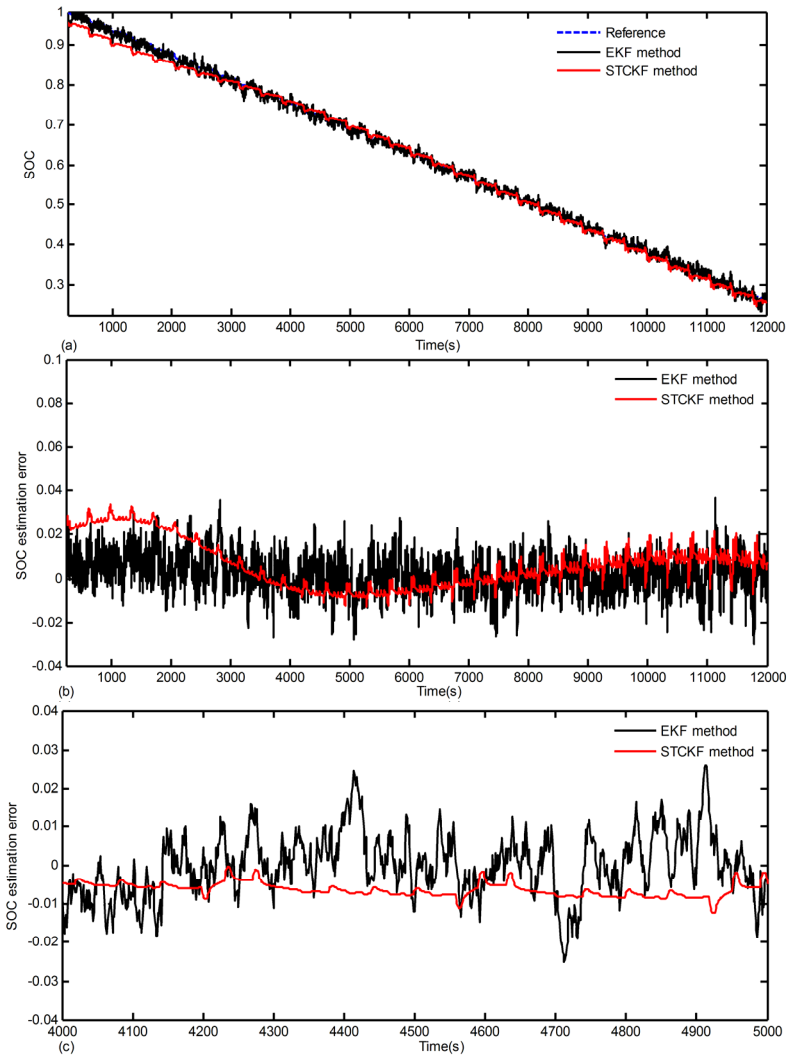

Figure 6. The estimation results under Dynamic Stress Test (DST): (**a**) SOC estimation profile; (**b**) SOC estimation error profile; and (**c**) Zoom plot of SOC estimation error profile.

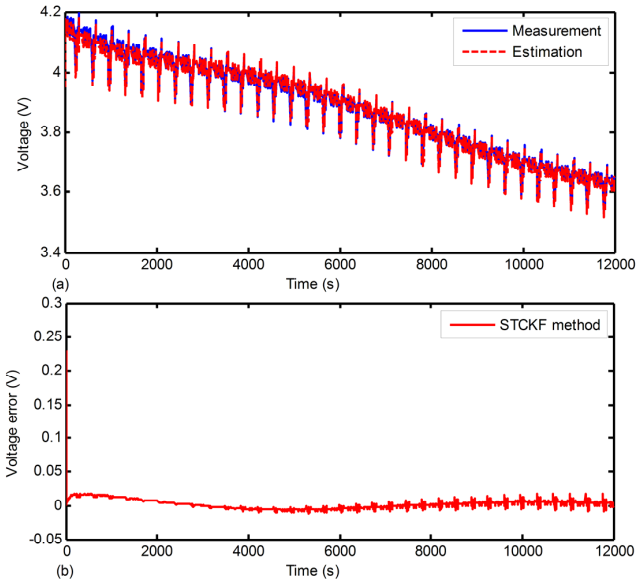

Figure 7. Terminal voltage estimation under DST: (**a**) Voltage profile; and (**b**) Voltage estimation error profile.

5.2. Estimation Results under New European Driving Cycle (NEDC) Cycle with Voltage Noise

In practice, it is difficult to always obtain the precise measurement of current and voltage, because of the noise interference caused by incorrect current and voltage sensor error and electromagnetic interference. In order to simulate the practical condition, a sequence of voltage noise was attached to measured voltage to verify the robustness of the developed method against measurement noise. The comparison with the frequently-used extended Kalman filter (EKF) and cubature Kalman filter (CKF) can show the characteristics in terms of accuracy and robustness. As is shown in Figure 8a, the absolute value of voltage noise is less than 0.08 V and Figure 8b illustrates more details.

The comparison results of SOC estimation are shown in Figure 9. As indicated in the Figure 9a, the black solid-line is the reference SOC value calculated by Coulomb counting method with accurate current values and initial SOC value, the red solid-line is SOC estimation using EKF method, the blue solid-line shows SOC estimation result by CKF method and the green solid-line represents the SOC estimation computed by STCKF method. From Figure 9b, it is clear that the SOC estimation error calculated by STCKF method has a smaller fluctuation than estimation error using EKF or CKF method. In order to further evaluate merits of the STCKF, the comparison of root mean square error (RMSE), maximum estimation error and execution time with different method are shown in Table 3. It is shown that the RMES of EKF method and CKF method are 0.0233 and 0.0157, respectively, while the RMSE computed by STCKF method is 0.0133. The maximum errors of EKF and CKF are 6.13% and 5.28%, respectively, while that of the STCKF is only 4.17%. As shown in Table 3, execution time of EKF method and CKF method are 0.89 and 1.55 s, respectively. However, execution time of STCKF method is 2.58 s. Therefore, it can be concluded that although the STCKF takes more computational cost, it is more robust to measurement noise compared with the EKF and CKF algorithms.

Table 3. Comparison of SOC estimation method under NEDC test.

Estimation Method	EKF	CKF	STCKF
RMSE	0.0233	0.0157	0.0133
Maximum error	6.13%	5.28%	4.17%
Execution time	0.89 s	1.55 s	2.58 s

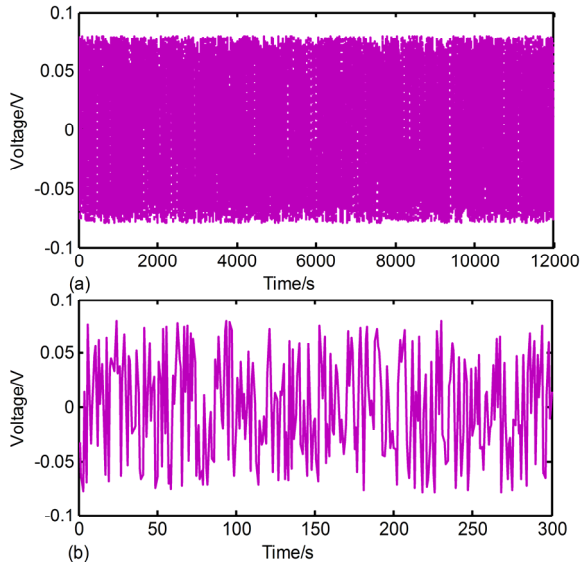

Figure 8. Random voltage noise: (**a**) Random noise profile; (**b**) Zoom plot of random noise profile.

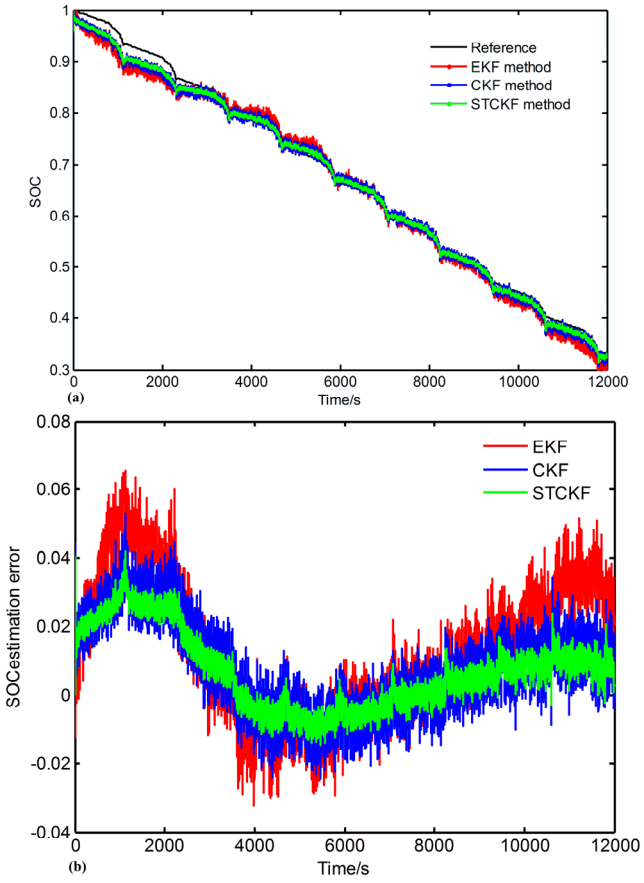

Figure 9. The SOC estimation results under New European Driving Cycle (NEDC) test: (**a**) SOC estimation profile; (**b**) SOC estimation error profile.

6. Conclusions

In this paper, the STCKF algorithm is proposed for SOC estimation of lithium-ion batteries in EVs. The STCKF algorithm is based on the cubature Kalman filter and satisfies the orthogonality

principle by introducing fading factor to the state estimation covariance matrix, improving the accuracy and robustness. The frequently-used second-order RC equivalent circuit model is selected to describe the nonlinear dynamic behaviors of lithium-ion batteries to realize the trade-off between computation cost and accurate dynamic characteristics. The exponential-function fitting method and sixth-order polynomial fitting are used to implement parameters identification. The Dynamic Stress Testing with 5% initial SOC error is applied to validate performance of STCKF algorithm. The experiment results of SOC and terminal voltage illustrate that the proposed method for SOC estimation performs well in terms of estimation accuracy and self-correction capability to initial SOC error. Furthermore, comparison with EKF and CKF method under NEDC cycle test with a sequence of voltage noise reveals the good property in SOC estimation accuracy and robustness. However, there are also some issues in the proposed method that need further investigations. Constant model parameters are applied to obtain SOC information and the SOC dependency of the model parameters is not studied.

Acknowledgments: This work is supported by the Shenzhen Key Laboratory of LED (light emitting diode) Packaging Funded Project (No. NZDSY20120619141243215).

Author Contributions: Bizhong Xia and Haiqing Wang developed the essential idea behind the present research and prepared the manuscript in the early stages. Mingwang Wang, Wei Sun, Yongzhi Lai and Zhihui Xu established the test bench and carried out the experiments. Final review, including final manuscript corrections, was done by Haiqing Wang.

Conflicts of Interest: The authors declare no conflict of interest.

References

1. Lu, L.; Han, X.; Li, J.; Hua, J.; Ouyang, M. A review on the key issues for lithium-ion battery management in electric vehicles. *J. Power Sources* **2013**, *226*, 272–288. [CrossRef]
2. Lotfi, N.; Fajri, P.; Novosad, S.; Savage, J.; Landers, R.G.; Ferdowsi, M. Development of an experimental testbed for research in lithium-ion battery management systems. *Energies* **2013**, *6*, 5231–5258. [CrossRef]
3. Ng, K.; Moo, C.S.; Chen, Y.P.; Hsieh, Y.C. Enhanced coulomb counting method for estimating state-of-charge and state-of-health of lithium-ion batteries. *Appl. Energy* **2009**, *86*, 1506–1511. [CrossRef]
4. Lee, S.; Kim, J.; Lee, J.; Cho, B.H. State-of-charge and capacity estimation of lithium-ion battery using a new open-circuit voltage *versus* state-of-charge. *J. Power Sources* **2008**, *185*, 1367–1373. [CrossRef]
5. Cheng, B.; Bai, Z.F.; Gao, B.G. State of charge estimation based on evolutionary neural network. *Energy Convers. Manag.* **2008**, *49*, 2788–2794.
6. Charkhgard, M.; Farrokhi, M. State-of-charge estimation for lithium-ion batteries using neural networks and EKF. *IEEE Trans. Ind. Electron.* **2010**, *57*, 4178–4187. [CrossRef]
7. Schwunk, S.; Armbruster, N.; Straub, S.; Kehl, J.; Vetter, M. Particle filter for state of charge and state of health estimation for lithium-iron phosphate batteries. *J. Power Sources* **2013**, *239*, 705–710. [CrossRef]
8. Shao, S.; Bi, J.; Yang, F.; Guan, W. On-line estimation of state-of-charge of Li-ion batteries in electric vehicle using the resampling particle filter. *Transp. Res. D Transp. Environ.* **2014**, *32*, 207–217. [CrossRef]
9. Barbarisi, O.; Vasca, F.; Glielmo, L. State of charge Kalman filter estimator for automotive batteries. *Control Eng. Pract.* **2006**, *14*, 267–275. [CrossRef]
10. Sepasi, S.; Roose, L.; Matsuura, M.M. Extended Kalman filter with afuzzy method for accurate battery pack state of charge estimation. *Energies* **2015**, *8*, 5217–5233. [CrossRef]
11. Sepasi, S.; Ghorbani, R.; Liaw, B.Y. A novel on-board state-of-charge estimation method for aged Li-ion batteries based on model adaptive extended Kalman filter. *J. Power Sources* **2014**, *245*, 337–344. [CrossRef]
12. Plett, G.L. Extended Kalman filtering for battery management systems of LiPB-based HEV battery packs Part 3. State and parameter estimation. *J. Power Sources* **2004**, *134*, 277–292. [CrossRef]
13. Xiong, R.; Gong, X.; Mi, C.C. A robust state-of-charge estimator for multiple types of lithium-ion batteries using adaptive extended Kalman filter. *J. Power Sources* **2013**, *243*, 805–816. [CrossRef]
14. Wan, E.; van der Merwe, R. The unscented Kalman filter for nonlinear estimation. In Proceedings of the IEEE 2000 Adaptive Systems for Signal Processing, Communications, and Control Symposium, AS-SPCC, Lake Louise, AB, Canada, 1–4 October 2000; pp. 153–158.

15. Tian, Y.; Xia, B.; Sun, W.; Xu, Z.; Zheng, W. A modified model based state of charge estimation of power lithium-ion batteries using unscented Kalman filter. *J. Power Sources* **2014**, *270*, 619–626. [CrossRef]
16. Zhang, W.; Shi, W.; Ma, Z. Adaptive unscented Kalman filter based state of energy and power capability estimation approach for lithium-ion battery. *J. Power Sources* **2015**, *289*, 50–62. [CrossRef]
17. Sun, F.; Hu, X.; Zou, Y.; Li, S. Adaptive unscented Kalman filtering for state of charge estimation of a lithium-ion battery for electric vehicles. *Energy* **2011**, *36*, 3531–3540. [CrossRef]
18. Dey, S.; Ayalew, B.; Pisu, P. Adaptive observer design for a Li-ion cell based on coupled electrochemical-thermal model. In Proceedings of the ASME Dynamic Systems and Controls Conference, San Antonio, TX, USA, 22–24 October 2014.
19. Dey, S.; Ayalew, B.; Pisu, P. Nonlinear robust observers for state-of-charge estimation of lithium-ion cells based on a reduced electrochemical model. *IEEE Trans. Control Syst. Technol.* **2015**, *23*, 1935–1942. [CrossRef]
20. Moura, S.; Krstic, M.; Chaturvedi, N. Adaptive PDE observer for battery SOC/SOH estimation via an electrochemical model. *J. Dyn. Syst. Meas. Control* **2013**, *136*. [CrossRef]
21. Arasaratnam, I.; Haykin, S. Cubature Kalman filters. *IEEE Trans. Autom. Control* **2009**, *56*, 1254–1269. [CrossRef]
22. Arasaratnam, I.; Haykin, S.; Hurd, T.R. Cubature Kalman filtering for continuous-discrete systems: Theory and simulations. *IEEE Trans. Signal Process.* **2010**, *58*, 4977–4993. [CrossRef]
23. Arasaratnam, I.; Haykin, S. Cubature Kalman smoothers. *Automatica* **2011**, *47*, 2245–2250. [CrossRef]
24. Dahmahi, M.; Meche, A.; Keche, M.; Oramri, A. Reduced cubature Kalman filtering applied to target tracking. In Proceedings of the 2nd International Conference on Control, Instrumentation and Automation (ICCIA), Shiraz, Iran, 27–29 December 2011; pp. 1097–1101.
25. Tang, X.J.; Liu, Z.B.; Zhang, J.S. Square-root quaternion cubature Kalman filtering for spacecraft attitude estimation. *Acta Astronaut.* **2012**, *76*, 84–94. [CrossRef]
26. Hu, X.S.; Li, S.B.; Peng, H. A comparative study of equivalent circuit models for Li-ion batteries. *J. Power Sources* **2012**, *198*, 359–367. [CrossRef]
27. Zhang, H.; Chow, M.Y. Comprehensive dynamic battery modeling for PHEV applications. In Proceedings of the IEEE Power and Energy Society General Meeting, Minneapolis, MN, USA, 25–29 July 2010; pp. 1–6.
28. Chen, M.; Rincon-Mora, G.A. Accurate electrical battery model capable of predicting runtime and I–V performance. *IEEE Trans. Energy Convers.* **2006**, *21*, 504–511. [CrossRef]
29. Tian, Y.; Chen, C.R.; Xia, B.Z.; Sun, W.; Xu, Z.H.; Zheng, W.W. An adaptive gain nonlinear observer for state of charge estimation of lithium-ion batteries in electric vehicles. *Energies* **2014**, *7*, 5995–6012. [CrossRef]
30. Schweighofer, B.; Raab, K.; Brasseur, G. Modeling of high power automotive batteries by the use of an automated test system. *IEEE Trans. Instrum. Meas.* **2003**, *52*, 1087–1091. [CrossRef]
31. Li, D.; Ouyang, J.; Li, H.; Wan, J. State of charge estimation for $LiMn_2O_4$ power battery based on strong tracking sigma point Kalman filter. *J. Power Sources* **2015**, *279*, 439–449. [CrossRef]
32. Wang, D.; Zhou, D.H.; Jin, Y.H.; Qin, S.J. A strong tracking predictor for nonlinear processes with input time delay. *Comput. Chem. Eng.* **2004**, *28*, 2523–2540. [CrossRef]
33. Xie, X.Q.; Zhou, D.H.; Jin, Y.H. Strong tracking filter based adaptive generic model control. *J. Process Control* **1999**, *9*, 337–350. [CrossRef]
34. Xia, B.; Wang, H.Q.; Tian, Y. State of charge estimation of lithium-ion batteries using an adaptive cubature kalman filter. *Energies* **2015**, *8*, 5916–5936. [CrossRef]